

Spin-orbit coupling induced fractionalized Skyrmion excitations in rotating and rapidly quenched spin-1 Bose-Einstein condensates

Chao-Fei Liu^{1,2} and Wu-Ming Liu¹

¹*Beijing National Laboratory for Condensed Matter Physics,*

Institute of Physics, Chinese Academy of Sciences, Beijing 100190, China and

²*School of Science, Jiangxi University of Science and Technology, Ganzhou 341000, China*

(Dated: April 11, 2012)

We investigate the fractionalized Skyrmion excitations induced by spin-orbit coupling in rotating and rapidly quenched spin-1 Bose-Einstein condensates. Our results show that the fractionalized Skyrmion excitation depends on the combination of spin-orbit coupling and rotation, and it originates from a dipole structure of spin which is always embedded in three vortices constructed by each condensate component respectively. When spin-orbit coupling is larger than a critical value, the fractionalized Skyrmions encircle the center with one or several circles to form a radial lattice, which occurs even in the strong ferromagnetic/antiferromagnetic condensates. We can use both the spin-orbit coupling and the rotation to adjust the radial lattice. The realization and the detection of the fractionalized Skyrmions are compatible with current experimental technology.

PACS numbers: 05.30.Jp, 03.75.Mn, 03.75.Lm

Introduction.—Spin-orbit coupling (SOC) describes the interaction of a particle's spin with its motion. The particular form of SOC can be of either Rashba [1] or Dresselhaus [2] type. SOC in an electronic system [3] is able to serve as a spin filter or a Stern-Gerlach apparatus. And it is crucial for the spin-Hall effect [4, 5] and topological insulators [6–9]. Recently, spin-orbit coupled Bose-Einstein condensate (BEC) has been realized in NIST's experiment [10] for the first time. Unlike previous experiment, their work has factually explored the bosons system in the non-Abelian gauge field [11–17]. This opens up a new avenue in cold atom physics and attracts many attentions.

Motivated by NIST's experiment [10], several recent investigations about bosons with SOC have presented some nontrivial new structures such as stripe phase [18–21] and half-quantum vortex state [20–22]. Specially, the combination effect of SOC and rotation on pseudo spin- $\frac{1}{2}$ BEC has been shown to be able to generate various vortex structures [23, 24]. These impressive results enrich the phase diagram of BEC system. However, how can SOC as a new effect on spinor BEC produce previously unknown types of topological excitations such as new Skyrmion?

In this Letter, we explore how SOC induces the fractionalized Skyrmions in rotating spin-1 BEC. We find that the fractionalized Skyrmion excitation which is related to a three-vortex structure exists in the rotating spin-1 BEC with SOC. Unlike previous Skyrmion-like excitations, the generation of the fractionalized Skyrmion excitation must depend on the combination of SOC and rotation. In the absence of rotation no fractionalized Skyrmion emerges, and this system can degenerate into the stripe phase. Without SOC, the integral Skyrmion excitations can appear in the ferromagnetic BECs. When SOC is larger than a critical value, the fractionalized Skyrmions encircle the center of the sys-

tem with one or several circles to form a radial lattice. These phenomena can occur even in the strong ferromagnetic/antiferromagnetic BECs. We can adjust the fractionalized Skyrmions lattice by changing the strength of SOC as well as rotation.

Model and equation.—Considered a quenching process, the dynamics of a spin-1 BEC can be described by the stochastic projected Gross-Pitaevskii equation [25–27]:

$$d\Psi_j = \mathcal{P}\left\{-\frac{i}{\hbar}\hat{H}_j\Psi_j dt + \frac{\gamma_j}{k_B T}(\mu - \hat{H}_j)\Psi_j dt + dW_j\right\}, \quad (1)$$

where Ψ_j ($j = 0, \pm 1$) denotes the macroscopic wave function of the atoms condensated in the spin state $|F = 1, m_F = j\rangle$, and $\hat{H}_j\Psi_j = [-\frac{\hbar^2\nabla^2}{2m} + V(r) + g_n|\Psi|^2]\Psi_j + g_s\sum_{\alpha=x,y,z}\sum_{n,k,l=0\pm 1}(\hat{F}_\alpha)_{jn}(\hat{F}_\alpha)_{kl}\Psi_n\Psi_k^*\Psi_l - \Omega\hat{L}_z\Psi_j + \kappa\sum_{\alpha=x,y}\sum_{n=0\pm 1}(\hat{F}_\alpha)_{jn}p_\alpha\Psi_n$, with the coupling constants $g_n = \frac{4\pi\hbar^2(2a_2+a_0)}{3m}$, $g_s = \frac{4\pi\hbar^2(a_2-a_0)}{3m}$ and the trap potential $V(r) = m\omega^2(x^2 + y^2)/2$. $\hat{F}_{\alpha=x,y,z}$ is the spin-1 matrix, Ω is the rotation frequency, \hat{L}_z [$\hat{L}_z = -i\hbar(x\partial_y - y\partial_x)$] is the z component of the orbital angular momentum, and κ denotes the strength of SOC. Meanwhile, T is the final temperature, μ is the chemical potential, γ_j is the growth rate for the j th component, and dW_j is the complex Gaussian noise. The projection operator \mathcal{P} is used to restrict the dynamics of the spinor BEC in the coherent region.

In numerical simulations, the initial state of each Ψ_j is generated by sampling the grand canonical ensemble for a free ideal Bose gas with the temperature T_0 and the chemical potential $\mu_{j,0}$. Meanwhile, the condensate band must lie below the energy cutoff $E_R > E_k = \frac{\hbar^2 k^2}{2m}$. Noting, $k = 2\pi(n_x, n_y)/L$, where n_x, n_y are integers and L is the size of the computation domain. To simulate the quenching process, the final temperature and the chemical potential of the noncondensate band are altered to

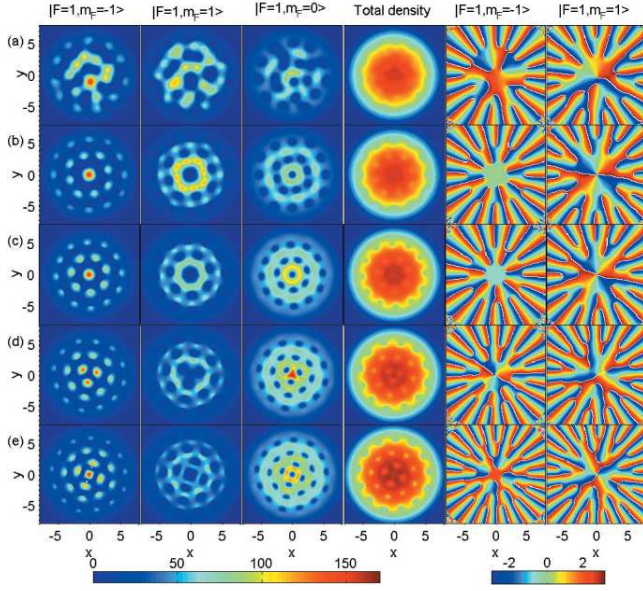


FIG. 1: (color online). The densities and phases for the spinor BEC of ^{87}Rb with SOC κ when the system reaches the equilibrium state. (a) $\kappa = 0.1$; (b) $\kappa = 0.2$; (c) $\kappa = 0.5$; (d) $\kappa = 0.7$; (e) $\kappa = 1.0$. Here, $\Omega = 0.5\omega$, $a_0 = 101.8a_B$ and $a_2 = 100.4a_B$. Noting, the fifth and sixth columns are the phases of $m_F = -1$ and $m_F = 1$ components, respectively.

the new values $T < T_0$ and $\mu > \mu_{j,0}$. Furthermore, we use the oscillator unit in the numerical computations. The length, time and energy are scaled in units of $\sqrt{\frac{\hbar}{m\omega}}$, ω^{-1} and $\hbar\omega$, respectively. In the simulations, the total number of the modes are $n_x, n_y = 300$, the energy cutoff is chosen at $n_{xc}, n_{yc} = 150$, the final temperature T is $10nK$, the chemical potential $\mu = 25\hbar\omega$, and $\frac{\gamma_i}{k_B T} = 0.03$.

Fractionalized Skyrmion lattice in rotating spin-1 BEC with spin-orbit coupling.—We begin with the spinor BEC of ^{87}Rb [28], which is ferromagnetic (FM) ($g_s < 0$). Figure 1 displays the densities and phases obtained under various strength of SOC. For a very weak SOC ($\kappa = 0.1$), the patterns are irregular. When κ is over 0.1, the patterns are relatively regular. The center of the systems displays various geometrical structures such as triangle, square, heptagon *etc.* These pictures factually display the transition of the patterns as the strength of SOC increases. Thus, SOC can be used to adjust the pattern in the rotating spin-1 BEC.

Just as previous experiments about the rotating BECs [25, 26], there are some vortices in the three components respectively. The fifth and sixth columns indicate the phases of $m_F = -1$ and $m_F = 1$ components respectively. Like the vortex lattice in single-component BEC, there are some lines where the phases change discontinuously from red to blue, which corresponds to the branch cuts between the phases $-\pi$ and π . The ends represent phase defects. All the lines extend to the outskirts of the BEC where the density of the BEC is almost negli-

ble, and end with another defect which offers neither the energy nor the angular momentum to the system. Furthermore, we also find some peaks accompanying the vortices, regularly arraying to be triangle, square, heptagon *etc.*, especially in the center of $m_F = -1$ component.

Unlike the periodic vortex lattice [25] or the vortices trimers [26], the vortices encircle the center with several circles. The number of vortices is 1 or 0 in the center, and it increases as the radius increases. Certainly, this phenomenon is not obvious when SOC is very weak ($\kappa = 0.1$). The fourth column shows the total density of BECs. Here, we can distinguish some local minimum of densities, especially when κ approaches 1.

To explore the possible Skyrmion structure, we further examine the spin texture [29, 30] which is parallel to the local magnetic moment. The spin texture is defined by $\mathbf{S}_\alpha = \sum_{m,n=0,\pm 1} \Psi_m^* (\hat{F}_\alpha)_{m,n} \Psi_n / |\Psi|^2$ ($\alpha = x, y, z$). Figure 2(a) shows the spin texture in Fig. 1(c). Here, the arrows form a Skyrmion-like circle only in the center of the system, namely the black pane region. By calculating the topological charge $Q = \frac{1}{4\pi} \int \mathbf{S} \cdot (\frac{\partial \mathbf{S}}{\partial x} \times \frac{\partial \mathbf{S}}{\partial y}) dx dy$, we find $Q = 1/2$ for the structure. Meanwhile, the arrows form big rings, whose main direction is marked with the blue arrows. But some mutations occur obviously, that is, the direction of arrow changes suddenly and the arrows form a small half circle locally. Additionally, the orientations of the arrows suffer a 180° reversal along the radius. For clarity, we use a blue pane to point out the special structure, where the topological charge is 0.25. There are many of these structures rounding the center with several circles, i.e., radially arranging in the system. We know the spin vector sweeps a whole unit sphere for a Skyrmion excitation with topological charge $Q = 1$; a half Skyrmion has the topological charge $Q = 1/2$, where the spin vector covers only half of a unit sphere [31]. Here, we find that the \mathbf{S} vector in the black pane covers half of a unit sphere, and the \mathbf{S} vector in the blue pane covers quarter of a unit sphere. Thus, we can call the two structures as half Skyrmion and fractionalized Skyrmion respectively. How do the half Skyrmion and the fractionalized Skyrmions emerge in this system? Why does it only cause one half Skyrmion?

Figure 2(b) illuminates the relationship between the vortices and the fractionalized Skyrmions. The green, blue and red spots are the center of vortices formed by $m_F = -1$, $m_F = 0$ and $m_F = +1$ components, respectively. Except for the central area of the BECs, we find the positions of vortices in the three components are far away from the center with certain order: green, blue and red. Meanwhile, the sequence distributes in the whole system. Thus, we can view the three-vortex structure as a cell. Undoubtedly, the number of vortices in the three components approaches 1 : 1 : 1. Furthermore, each fractionalized Skyrmion accompanies a three-vortex structure. Usually, the Skyrmion-like excitations [29, 30] are related to the underlying vortex configuration such

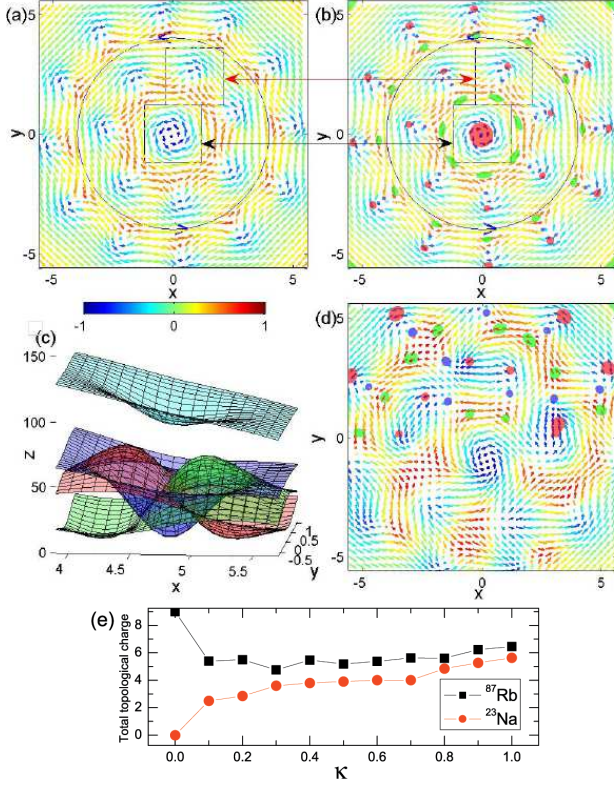


FIG. 2: (color online). (a) Spin texture of spinor BEC of ^{87}Rb with $\kappa = 0.5$ and $\Omega = 0.5\omega$. The color of each arrow indicates the magnitude of S_z . The black pane points out a half Skyrmion, and the blue pane indicates a fractionalized Skyrmion. The blue arrows show the main direction of the spin texture. (b) The position of vortices and the spin texture. The green, blue and red spots are the center of vortices formed by the $m_F = -1$, $m_F = 0$ and $m_F = +1$ components, respectively. (c) A scheme of three-vortex structure. The green, blue and red surfaces denote the densities of the $m_F = -1$, $m_F = 0$ and $m_F = +1$ components, respectively. The cyan is the total density of the BECs. (d) The position of vortices and the spin texture of spinor BEC of ^{87}Rb with $\kappa = 0.1$ and $\Omega = 0.5\omega$. Noting, we only mark the vortices in $y > 0$ region in order to illuminate the spin texture and position of vortices clearly. (e) The total topological charge of system under the equilibrium state as a function of SOC strength κ , where $\Omega = 0.5\omega$.

as Mermin-Ho [32] and Anderson-Toulouse [33] vortices. Here, the fractionalized Skyrmion is related to the three-vortex structure.

Figure 2(c) further indicates a scheme of the three-vortex structure with the density distribution. Here, the green, blue and red surfaces represent the densities of the $m_F = -1$, $m_F = 0$ and $m_F = +1$ components, respectively. The cyan represents the total density. There is a local density minimum at the position of vortex formed by $m_F = 0$ component when we examine the total density. This point is different from the normal coreless vortex [29, 30, 32, 33] where the total density has no singu-

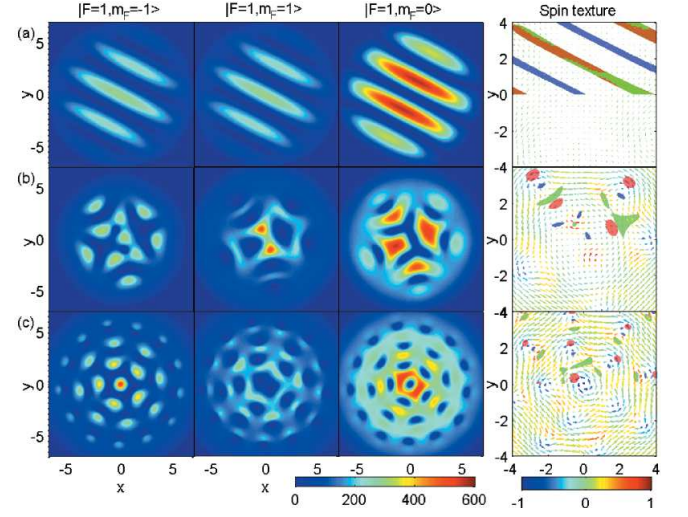


FIG. 3: (color online). The effect of rotation frequency Ω for spinor BEC of ^{23}Na with $\kappa = 1$, $a_0 = 50a_B$ and $a_2 = 55a_B$. (a) $\Omega = 0$; (b) $\Omega = 0.2\omega$; (c) $\Omega = 0.5\omega$. The fourth column shows the corresponding spin textures and position of vortices. The meanings of the spots and the colored arrows are the same as those in Fig. 2(b). Noting, we only mark the vortices in $y > 0$ region.

larity. The $m_F = +1$ component forms a obvious hump at the vortex region of $m_F = -1$ component, and vice versa. Those properties cause a dipole of spin. Generally, the dipole is embedded in the three-vortex structure.

In the absence of SOC, the periodic Skyrmion lattice can be created in the rotating spin-1 BEC of ^{87}Rb [26]. Figure 2(d) shows the spin textures and the position of vortices when the strength of SOC is 0.1. Here, the vortices hardly form the three-vortex structure, especially near the center. Additionally, the fractionalized Skyrmion lattice is not very obvious. These results further prove that the fractionalized Skyrmion is related to the three-vortex structure. The distribution of fractionalized Skyrmion depends on that of vortices. Thus, it is not inconceivable that the different strength of SOC will cause various fractionalized Skyrmion lattices.

Figure 2(e) shows that the total topological charge of the system varies as SOC is increasing. Because SOC changes the integral Skyrmions into the fractionalized ones, the total topological charge of FM BECs tends to decrease firstly. Then, the value generally gets greater. Furthermore, we find the fractionalized Skyrmion lattice can also occur in the antiferromagnetic (AFM) BEC, where $g_s > 0$ [see Fig. 3(c)]. There is no Skyrmion excitation appearing in rotating AFM BEC of ^{23}Na [26] when $\kappa = 0$ (the total topological charge is 0 in Fig. 2(e)). Added SOC, the total topological charge increases. This means that SOC enhances the fractionalized Skyrmion excitations. Especially, to obtain the fractionalized Skyrmion lattice, the strength of SOC must exceed a critical value. Here, this value approaches 0.2.

The effect of the rotation frequency.—Here, we use the spinor BEC of ^{23}Na to illustrate the effect of the rotation frequency. We only change the rotation frequency Ω and fix all other parameters to perform the numerical experiments. Figure 3 shows the density distribution and spin texture under various rotation frequencies. In the absence of rotation ($\Omega = 0$), there is no vortex appearing at all. Each component of the BECs is split to be several parallel parts. In fact, these properties agree with the stripe phase [18–21]. The spin texture indicates no fractionalized Skyrmion excitations in this system. The color straps factually are the low density domain of BECs. Added a weak rotation (0.2ω), the splitting parts bend and break, and several vortices and the three-vortex structure occur. When the rotation becomes faster (0.5ω), the vortex lattice emerges and the fractionalized Skyrmion lattice is very obvious. Naturally, the rotation can control the fractionalized Skyrmion lattice because it can induce the underlying vortices.

Now, we can systematically understand the above questions. Its dynamics is driven by the rotation in the quenching process and the intrinsic spin-Hall effect derived from the effective SOC. As is well known in the study of rotating superfluid helium [34, 35], the rotating drive pulls vortices into the rotation axis, while repulsive interaction tends to push them apart; this competition yields a vortex lattice whose vortex density depends on the rotation frequency. Meanwhile, the SOC causes the spin separation and creates the dipole structure of spin, which is embedded in the three-vortex structure. The fractionalized Skyrmion derives from the dipole structure. In term of densities, only a core structure appears in the center. That is the origin of the single half Skyrmion. Noting that the core structure of densities agrees with the densities distribution of half Skyrmion in experiment [36].

The effect of tuning the ferromagnetic and antiferromagnetic interactions.—Generally speaking, g_s is much smaller than g_n . By adjusting the two s -wave scattering lengths a_0 and a_2 through Feshbach resonances, the spin exchange interaction strength g_s is tunable. We now perform the above experiments by changing a_2 . Figures 4(a1)-(d1) show a stronger FM case of ^{87}Rb ($g_s/g_n = -0.255$). Contrasting the densities and the spin texture, we find the three-vortex structure and the fractionalized Skyrmion lattice are common in this FM BEC, though there are several half Skyrmions near the center. Furthermore, we also test a stronger AFM BEC of ^{23}Na ($g_s/g_n = 0.222$). The three-vortex structure and the fractionalized Skyrmion mainly emerge at the outskirt of the BECs. In fact, the strong AFM interactions restrict the fractionalized Skyrmion excitations, so the fractionalized Skyrmion hardly emerges in the center. These experiments show the universality of the fractionalized Skyrmion excitation in BEC with SOC.

Conclusion.—We have found a new type of topological

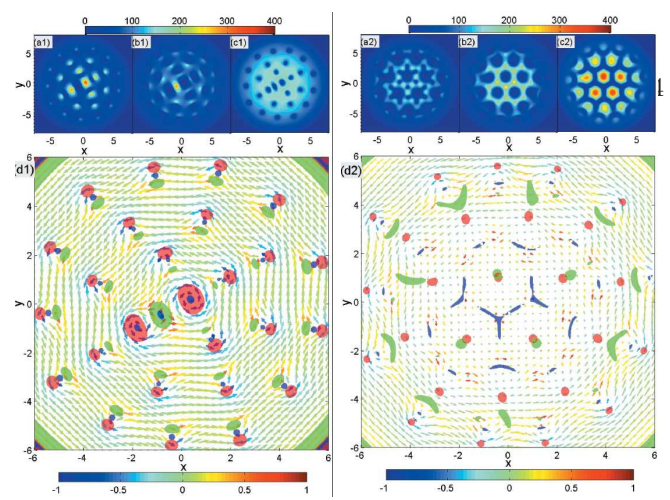


FIG. 4: (color online). The effect of tuning FM and AFM interactions for BEC with $\kappa = 1$ and $\Omega = 0.5\omega$. (a1), (b1) and (c1) show the densities of the $m_F = -1$, $m_F = 1$ and $m_F = 0$ components of ^{87}Rb with $a_0 = 101.8a_B$ and $a_2 = 50.2a_B$ respectively (strong FM case); (d1) shows the spin texture and the position of vortices. The meanings of the spots and the colored arrows are the same as those in Fig. 2(b). (a2)-(d2) indicate the corresponding results of ^{23}Na with $a_0 = 50a_B$ and $a_2 = 110a_B$ (strong AFM case).

excitation—fractionalized Skyrmion—in the rotating spin-1 BEC with SOC. The fractionalized Skyrmion originates from a dipole resulted from a local spin separation. The fractionalized Skyrmion excitation can occur as long as the three-vortex structure appears, even in the strong FM and AFM BEC with SOC. Our study gives an experimental protocol to observe these novel phenomena in future experiments. Not only do our findings exist in spin-1 BEC, but also the related textures should appear in high-spin BEC, superfluid and superconduction. This work is of particular significance for exploring the novel topological excitation such as fractionalized Skyrmions in quantum gas and condensed matter physics.

We are grateful to S.-C. Gou for useful comments. This work was supported by the NKBRSCF under grants Nos. 2011CB921502, 2012CB821305, 2009CB930701, 2010CB922904, and NSFC under grants Nos. 10934010, 60978019, and NSFC-RGC under grants Nos. 11061160490 and 1386-N-HKU748/10.

-
- [1] Y. A. Bychkov and E. I. Rashba, J. Phys. C **17**, 6039 (1984).
 - [2] G. Dresselhaus, Phys. Rev. **100**, 580 (1955).
 - [3] A. M. Dudarev, R. B. Diener, I. Carusotto, and Q. Niu, Phys. Rev. Lett. **92**, 153005 (2004).
 - [4] Y. K. Kato *et al.*, Science **306**, 1910 (2004).
 - [5] M. König *et al.*, Science **318**, 766 (2007).
 - [6] C. L. Kane and E. J. Mele, Phys. Rev. Lett. **95**, 146802 (2005).
 - [7] B. A. Bernevig *et al.*, Science **314**, 1757 (2006).
 - [8] D. Hsieh *et al.*, Nature **452**, 970 (2008).
 - [9] K. Sun, W. V. Liu, A. Hemmerich and S. D. Sarma, Nature Physics, **8**, 67 (2012).

- [10] Y.-J. Lin *et al.*, Nature **471**, 83 (2011).
- [11] J. Ruseckas, G. Juzeliunas, P. Öhberg, and M. Fleischhauer, Phys. Rev. Lett. **95**, 010404 (2005).
- [12] K. Osterloh, M. Baig, L. Santos, P. Zoller, and M. Lewenstein, Phys. Rev. Lett. **95**, 010403 (2005).
- [13] I. I. Satija, D. C. Dakin, and C. W. Clark, Phys. Rev. Lett. **97**, 216401 (2006).
- [14] S. L. Zhu, H. Fu, C. J. Wu, S. C. Zhang, and L. M. Duan, Phys. Rev. Lett. **97**, 240401 (2006).
- [15] X. J. Liu, X. Liu, L. C. Kwek, and C.H. Oh, Phys. Rev. Lett. **98**, 026602 (2007).
- [16] T. D. Stanescu, C. Zhang, and V. Galitski, Phys. Rev. Lett. **99**, 110403 (2007).
- [17] G. Juzeliunas, J. Ruseckas, and J. Dalibard, Phys. Rev. A **81**, 053403 (2010).
- [18] C. Wang, C. Gao, C.-M. Jian, and H. Zhai, Phys. Rev. Lett. **105**, 160403 (2010).
- [19] T.-L. Ho and S. Z. Zhang, Phys. Rev. Lett. **107**, 150403 (2011).
- [20] C.-M. Jian and H. Zhai, Phys. Rev. B **84**, 060508(R) (2011).
- [21] S. Sinha, R. Nath, and L. Santos, Phys. Rev. Lett. **107**, 270401 (2011).
- [22] H. Hu, B. Ramachandhran, H. Pu, and X.-J. Liu, Phys. Rev. Lett. **108**, 010402 (2012).
- [23] X.-Q. Xu and J. H. Han, Phys. Rev. Lett. **107**, 200401 (2011).
- [24] X.-F. Zhou, J. Zhou, and C. Wu, Phys. Rev. A **84**, 063624 (2011).
- [25] A. S. Bradley, C. W. Gardiner, and M. J. Davis, Phys. Rev. A **77**, 033616 (2008).
- [26] S.-W. Su *et al.*, Phys. Rev. A **84**, 023601 (2011).
- [27] S. J. Rooney, A. S. Bradley, and P. B. Blakie, Phys. Rev. A **81**, 023630 (2010).
- [28] F. Zhou, Phys. Rev. Lett. **87**, 080401 (2001).
- [29] T. Mizushima, K. Machida, and T. Kita, Phys. Rev. Lett. **89**, 030401 (2002); T. Mizushima, N. Kobayashi, and K. Machida, Phys. Rev. A **70**, 043613 (2004).
- [30] K. Kasamatsu, M. Tsubota, and M. Ueda, Phys. Rev. Lett. **93**, 250406 (2004); K. Kasamatsu, M. Tsubota, and M. Ueda, Phys. Rev. A **71**, 043611 (2005).
- [31] U. Leonhardt and G. E. Volovik, JETP Lett. **72**, 46 (2000).
- [32] N. D. Mermin and T.-L. Ho, Phys. Rev. Lett. **36**, 594 (1976).
- [33] P. W. Anderson and G. Toulouse, Phys. Rev. Lett. **38**, 508 (1977).
- [34] L. J. Campbell and R. M. Ziff, Phys. Rev. B **20**, 1886 (1979).
- [35] M. Tsubota and H. Yoneda, J. Low Temp. Phys. **101**, 815 (1995).
- [36] A. E. Leanhardt, Y. Shin, D. Kielpinski, D. E. Pritchard, and W. Ketterle, Phys. Rev. Lett. **90**, 140403 (2003).